

ILIKON CORPORATION
NATICK, MASSACHUSETTS

FACILITY FORM 802

N 65 15189

(ACCESSION NUMBER)

50

(PAGES)

CP 60225

(NASA CR OR TMX OR AD NUMBER)

(THRU)

(CODE)

17

(CATEGORY)

BASIC STUDIES
ON
DISPERSION HARDENING

Dr. Robert Grierson

FINAL REPORT
Contract No. NASw-726

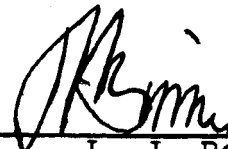
GPO PRICE \$ _____

OTS PRICE(S) \$ _____

Hard copy (HC) 2.00

Microfiche (MF) .50

APPROVED:



L. J. Bonis
Technical Director

April 10, 1964

ABSTRACT

15189

An investigation of the elastic strains associated with the particle-matrix interface in certain dispersion strengthened alloys] has been carried out. Two techniques have been used to observe these strains. These techniques involve the measurement of diffraction contrast effects as observed using transmission electron microscopy and the measurement of the broadening of x-ray diffraction lines.

author

TABLE OF CONTENTS

	<u>Page No.</u>
1. Introduction	1
2. The Measurement of Elastic Strains by Using Transmission Electron Microscopy	2
3. The Measurement of Elastic Strains by Using X-Ray Diffraction Techniques	8
4. The Origins of the Elastic Strains which Exist at the Particle-Matrix Interface in Dispersed Phase Alloys	11
5. Material Preparation	15
6. Results	18
7. Discussion	25
8. References	27
9. Tables	29

1.

INTRODUCTION

The work currently being reported is a study of the elastic strains in dispersion strengthened alloys. In particular, the research has concerned itself with those elastic strains which are associated with the dispersed phase particle - matrix interface. It is thought that the existence of these strains may be one of the prime reasons for the high strength of dispersion strengthened materials. It is also thought that they may have a considerable effect on the high temperature stability of the alloys under investigation.

Four alloy systems have been examined. All materials were prepared by the internal oxidization of dilute binary solid solutions of various elements in nickel. Two techniques have been used to measure the strains in these materials. These techniques involve the measuring of:

- (1) The diffraction contrast effects
as observed using transmission
electron microscopy.
- (2) The broadening of x-ray diffraction
lines.

2. THE MEASUREMENT OF ELASTIC STRAINS BY USING
 TRANSMISSION ELECTRON MICROSCOPY

a) Introduction

Various types of finely divided dispersions in metallic matrices have been investigated using electron diffraction and transmission electron microscopy. It has been found that, when a strain is associated with the particle-matrix interface, a certain diffraction contrast effect can be observed. Essentially, the contrast effect is that a pair of D-shaped lobes symmetrically placed about a line of no contrast, which, when one strong reflection is operating, is perpendicular to the reciprocal lattice vector corresponding to the reflection. The contrast effect is visible only when one or more sets of lattice planes diffract strongly, and will disappear when the foil is tilted away from this position. As will be subsequently described, this diffraction effect can be predicted by using the dynamical theory of electron diffraction.

Diffraction effects of the type described above were first observed in precipitation strengthened alloys. Becher,⁽¹⁾ Bean and Livingston⁽²⁾ and Phillips and Livingston⁽³⁾ have observed them in the copper-cobalt system. The theoretical prediction of the diffraction contrast effect, made by Ashby and Brown,⁽⁴⁾ was made using the copper-cobalt system as a model. In this case, the interfacial strains are due to coherency between the particles and the matrix.

The concept of strained interface contrast effects was then applied to internally oxidized copper-aluminum and copper-silicon alloys by Ashby and Brown.⁽⁵⁾ In this case they extended their previously stated theory to cover strains due to the presence of non-coherent particles. Ansell and Goodrich⁽⁶⁾ have observed the D-shaped contrast effects in association with γ -alumina particles in SAP alloys. They report that the existence of strains also results in the streaking of the selected area electron diffraction pattern. This streaking occurs in the direction of the reciprocal lattice vector, g , of the reflection operating.

b) Theory

The theory of diffraction contrast from the strained particle-matrix interface may be developed from the dynamical theory of electron diffraction contrast as derived by Howie and Whelan⁽⁷⁾ for the simple case of a spherically symmetrical strain field. This development is the work of Ashby and Brown.⁽⁴⁾

For an elastic inclusion in an isotropic matrix the radial displacement of the matrix, u , can be written

$$u = \epsilon r$$

where r is the distance from the center of the particle and ϵ is a parameter describing the elastic strain field. When the

inclusion is larger than the volume of matrix it displaces (interstitial inclusions), then ϵ is positive.

The basic equations describing the amplitude of the transmitted beam, A_0 , and that of the diffracted beam, A_g , as a function of depth, z , in the crystal (using the column approximation where only small changes in amplitude and phase are assumed between neighboring columns) are:

$$\frac{d A_0}{dz} = - \frac{\pi}{X_{0'}} A_0 + \pi \left(\frac{1}{X_g} - \frac{1}{X_{g'}} \right) A_g$$

$$\frac{d A_g}{dz} = \pi \left(\frac{1}{X_g} - \frac{1}{X_{g'}} \right) A_0 + \left(- \frac{\pi}{X_{0'}} + 2\pi i (S_g + \beta') \right) A_g$$

where

$$\beta' = \frac{d}{dz} (\bar{g} \cdot \bar{u})$$

The predicted transmitted and diffracted intensities are, of course, $|A_0|^2$ and $|A_g|^2$ respectively. X_g is the extinction distance corresponding to diffraction from the reciprocal lattice planes whose vector is \bar{g} and is essentially the distance the direct beam must travel in the column of crystal before the diffracted intensity becomes appreciable and hence double diffraction becomes important. The absorption parameters $\frac{X_g}{X_{0'}}$ and $\frac{X_g}{X_{g'}}$ describe the decay of

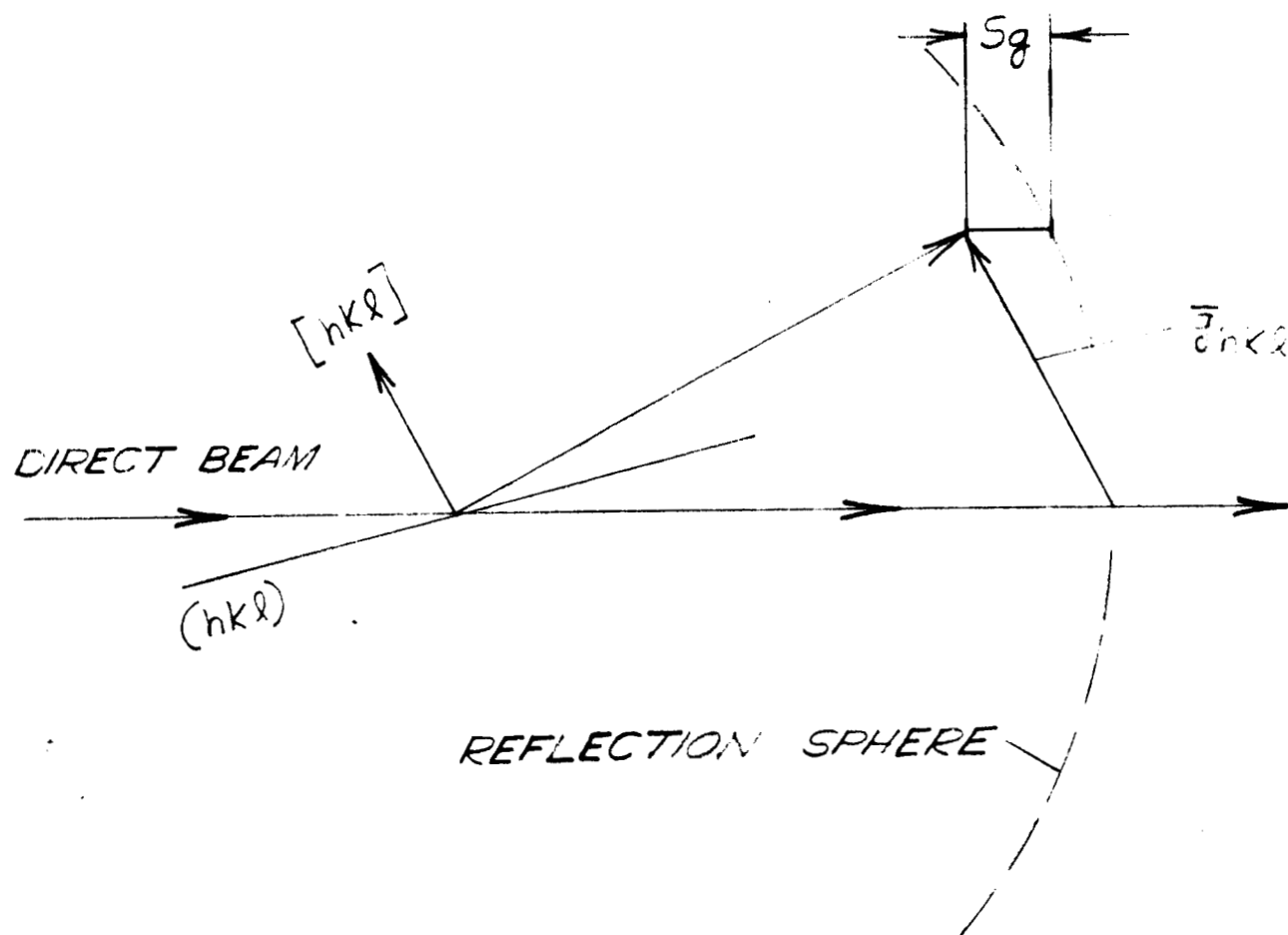
transmitted and diffracted intensities and the bright field extinction contours (the so-called anomalous absorption) respectively.

Absorption cannot be considered constant with foil thickness. (This is the assumption underlying the Kinematical Theory and is only good when the diffracted intensity is very small when compared with the direct intensity, a situation which does not apply to the current problem at all.)

S_g is a parameter defining the deviation from the Bragg angle, and is equal to the distance from the reciprocal lattice point \vec{g} to the reflection sphere measured parallel to the direct beam (see diagram over).

S_g is taken to be positive when the reciprocal lattice point is inside the sphere. The width of the image, defined as a fractional intensity variation over background, varies with S_g and has a maximum at $S_g = 0$ (where the Bragg angle is exactly fulfilled). Experimentally, it is best to photograph bend contours on the foil where an area can be chosen such that $S_g = 0$ since non-zero values are difficult to estimate.

Ashby and Brown have used a computer to integrate the basic equations down columns of the crystal starting with $A_0 = 1$ and $A_g = 0$ at $z = 0$. The transmitted and diffracted intensities were evaluated as a function of position in the column. They made the following transformations to render the variables dimensionless:



$$W = S_g X_g; \text{ thickness } T = \frac{t}{X_g}; \text{ inclusion radius } R_o = \frac{r_o}{X_g};$$

$$\text{and the depth of the inclusion from the foil surface } V = \frac{v}{X_g}.$$

Thus all variables are expressed in terms of the extinction distance.

In the matter of defining image width, it must be realized that these contrast effects have no sharply delineated boundaries. Ashby and Brown therefore define a "2% width" where the intensity of the diffraction contrast is 2% different than that of the background. This is obviously the outermost periphery of the contrast effect which can be clearly discerned. They similarly define a 20% width and 50% width for purposes of mapping iso-intensity plots.

The dimensionless parameter

$$\frac{\epsilon \bar{g} r_o^3}{X_g^2}$$

is seen to be the principal factor in the computation of image width. Ashby and Brown⁽⁴⁾ have published their results of the

dependence of image width/ X_g as a function of $\log \left(\frac{\epsilon \bar{g} r_o^3}{X_g^2} \right)$

in the form of a plot for 2%, 20% and 50% image widths; thus if one has fulfilled the diffraction conditions outlined above regarding Bragg angle, operating reflection, depth of inclusion

in the foil, etc., an estimate of ϵ can be made by measuring image width and inclusion radius from the micrograph, \bar{g} from the diffraction pattern and computing X_g for the reflections.

3. THE MEASUREMENT OF ELASTIC STRAINS BY USING X-RAY DIFFRACTION TECHNIQUES

In recent years considerable advances⁽⁸⁾ have been made in our ability to extract meaningful data from measurements of the profile of x-ray diffraction lines. Several authors^(9, 10, 11) have used these techniques to measure the internal strains in crystalline materials. The theory of the technique used in this case is briefly outlined below.

The shape of the x-ray diffraction line which we observe is controlled by two factors. One is the x-ray optics of the instrument which is being used to produce and measure the diffraction line in question, and the other is the degree of crystalline perfection of the material under observation. Departure from perfection in either case will cause an increase in the width of the diffraction line.

When an x-ray diffraction line is broadened by two different effects (or group of effects), then the variation of intensity across this line which occurs due to the presence of both effects $[h(x)]$ is related to the variation which would occur if these effects are present individually $[g(x) \text{ and } f(x)]$ by an equation of the form:

$$h(x) = \int f(y) g(x - y) dy \quad (1)$$

Let us call $f(x)$ the effect of crystalline imperfection and $g(x)$ the x-ray optical effect. We measure $h(x)$ directly

and if we can find $g(x)$ then we can, using the method described below, compute $f(x)$. We find $g(x)$ by using a specimen which gives negligible line broadening due to its own imperfection. The calculation of $f(x)$ is carried out in the following way.

The functions $f(x)$, $g(x)$ and $h(x)$ can all be represented by Fourier series of the form:

$$f(x) = \sum_{t=-\infty}^{+\infty} F_t e^{\frac{-2\pi i x t}{a}} \quad \text{etc.} \quad (2)$$

By substituting equation (2) into equation (1) and then suitably manipulating the resulting equation, we can obtain F_t in terms of G_t and H_t .

A computer program has been written which allows us to calculate G_t and H_t from the measured values of $g(x)$ and $h(x)$. Using these calculated values we are able to find a set of values of F_t . It is these values of F_t which we use to determine the elastic strains within the specimen under observation.

The above is a purely mathematical analysis of the shape of the x-ray diffraction lines. That the values of F_t have a physical meaning has been shown by Warren and Averbach.^(12, 13) In the case under consideration, F_t can be considered as the product of two components, F_t^D and F_t^S . F_t^D is due to the size of the coherently diffracting zones within the sample and F_t^S is due to the presence of elastic strains within the specimen. It has been shown⁽¹²⁾ that F_t^D is independent of

the order of the diffraction line, whereas F_t^S is dependent on the order of the diffraction line. We can, therefore, write:

$$F_t(l_o) = F_t^D \cdot F_t^S(l_o)$$

where $l_o (= \sqrt{h^2 + k^2 + l^2})$ is the order of the line. By considering the variation of $F_t(l_o)$ with l_o , we can thus separate the effect of domain size and elastic strain.

It has been shown that:

$$F_t^S(l_o) \propto e^{\frac{-2\pi^2 l_o^2 (\Delta L)^2}{a^2}}$$

where ΔL is the change in spacing of two planes of the set l_o due to the existence of elastic strains. In general, ΔL will be a function of L - the distance over which ΔL is measured. Following the method of McKeehan and Warren⁽¹⁴⁾ it is thus possible to find the variation with distance of the internal strains. To find if the strains are orientation dependent, we examine the plot of $F_t(l_o)$ against l_o . For a set of diffraction lines of the type (100) (200) (300), this will be a straight line. If it is the same straight line for all sets of diffraction lines, then there is no orientation dependence, if it is not, then an orientation dependence exists. In this way we can map the magnitude, range and orientation of the internal strains in a crystalline solid.

4. THE ORIGINS OF THE ELASTIC STRAINS WHICH EXIST
AT THE PARTICLE-MATRIX INTERFACE IN DISPERSED PHASE ALLOYS

In dispersed phased Ni base alloys, the interfacial elastic strains may be divided into three groups. These are:

- 1) Those due to the volume changes which occur during the formation and subsequent heat treatment of the alloys.
- 2) Those due to the existence of coherency between the particle and matrix.
- 3) Those due to the existence of various types of dislocations at the particle-matrix interface.

In the first group we have volume changes due to:

- (a) The formation of the dispersed phase from the parent solid solution.
- (b) Possible allotropic transformations of the dispersed phase (e.g., $\gamma \text{Al}_2\text{O}_3 \rightarrow \alpha \text{Al}_2\text{O}_3$).
- (c) Differences in the coefficient of thermal expansion of the dispersed phase and the matrix.

Volume changes due to causes (a) and (b) would occur at temperatures where diffusion would be sufficiently rapid to transport enough material to fully compensate for them. Changes due to (c), especially in material which has been quenched from a high temperature, would not usually be completely compensated

for in this way and so could cause elastic strains.

The second group covers the existence of elastic strains due to the localized adjustments of atomic position which are necessary to allow coherency to occur between a set of planes in the matrix and a set of planes, of slightly differing interplanar spacing, in the dispersed phase.

Dislocations which have differing origins may occur at the particle-matrix interface. First of all, in partially coherent systems, structural dislocations which allow the existence of some coherency may exist. Secondly, in those alloys where large elastic strains exist, plastic deformation to relieve these strains may occur. Thirdly, the diffusion of vacancies or interstitials in order to relieve volume changes may cause the formation of dislocation loops about the particles. Fourthly, during the preparation of the alloys, the deformation of the alloys may cause dislocations to pile up against the particles. How we hope to distinguish between these different causes of strain will be described later.

In the examination of precipitation strengthened alloys, the existence of coherency has been found⁽¹⁵⁾ to have a considerable effect on the strength of the alloy. A way in which coherency could occur in many dispersion hardened alloys is described below.

Coherency, in the precipitation strengthened alloys which have so far been investigated, occurs by the direct transition

from the matrix to the particle lattice. For this to be possible, only a small difference in lattice parameters between the two sets of coherent planes may exist. If, however, it is assumed that, in the region of the interface, some transitional structure exists, then coherency is much more likely to occur. Although these transitional structures do not need to be those of known compounds, they could be. A proposed way in which the structure, in the transitional region, may vary is described below.

We will first of all consider a transition from NiO to $\gamma\text{-Al}_2\text{O}_3$. It has previously been shown⁽¹⁶⁾ that if NiO and $\alpha\text{-Al}_2\text{O}_3$ are placed in contact and then heated, a compound with the formulae NiAl_2O_4 is formed. The structure of this compound is shown in Figure 3. The orientation of the NiAl_2O_4 was found to be controlled by that of the $\alpha\text{-Al}_2\text{O}_3$. It is possible that similar behavior would occur if γ rather than α -alumina were used. $\gamma\text{-Al}_2\text{O}_3$ and NiAl_2O_4 have identical atomic arrangements of their oxygen sub lattices and the oxygen-oxygen interatomic distance is less than 2% greater in the spinel than in the alumina (Figures 3 and 4). Coherency from NiO to $\gamma\text{-Al}_2\text{O}_3$ can, therefore, exist.

The formation of Al_2O_3 , at the temperature of γ stability, in internally oxidized Ni-Al solid solutions, is dependent on the diffusion of oxygen through the Ni lattice. This diffusion is predominantly interstitial. The crystal structure of nickel

oxide can be considered as that of Ni containing oxygen atoms in its interstices (see Figures 1 and 2). It is, therefore, probable that a continuous transformation from Ni to NiO can occur. In Figure 5, the transformation of the lattice from that of Ni to that of $\gamma\text{Al}_2\text{O}_3$ is shown.

5.

MATERIAL PREPARATION

Of the four alloy systems which have been examined, three ($\text{Ni-Al}_2\text{O}_3$, Ni-TiO_2 , Ni-SiO_2) were formed by the internal oxidation of the relevant binary solid solutions, while the fourth alloy (Ni-ThO_2) was obtained commercially. Two compositions of each of the first three alloys were prepared. One composition had a higher and the other a lower oxide content. The following technique was used.

Chips of the solid solution alloys were ball milled until they were reduced to a -270 mesh powder. This powder was then internally oxidized in a Lindberg tube furnace. The proper amount of oxygen was provided by a mixture of Ni-NiO (1:8 ratio) powder. All internal oxidation treatments were carried out at 750°C (in low oxygen partial pressures). The powders were then hydrogen reduced to eliminate all traces of NiO which may have been formed on the alloy particles, and the furnace cooled under hydrogen.⁽¹⁷⁾

In order to fabricate the internally oxidized powders, they were packed into a rubber hose and hydrostatically pressed at 30,000 psi. After pressing, the billets were once again hydrogen reduced in a double reduction process to eliminate any nickel oxide which may have formed during packing. The billets were then sintered in the same environment at 900°C for eight hours, after which the sintered billets were canned and extruded at a ratio of 1:40 and at a temperature of 1100°C .

The final specimen size was about 0.3" diameter in cross section. A sample of pure nickel powder (-270 mesh) was prepared in the same way. This nickel was used for comparison purposes. Table I is a list of the composition, particle size and particle distribution of the alloys used.

Thin films, approximately .015" thick, were prepared from the extruded rod by alternately rolling and annealing at 600°C. These films were then thinned electrolytically in order to give specimens on which transmission electron microscopy could be carried out. Somewhat thicker films were prepared, in a similar manner, for use in the x-ray line broadening work.

Two different electropolishing solutions were used to thin the internally oxidized nickel alloys. The first⁽¹⁸⁾ was of the composition:

Orthophosphoric acid ($d = 1.69$)	330 c.c.
Sulfuric acid ($d = 1.84$)	83 c.c.
Chromic acid (CrO_3)	18 grams
H_2O	42 c.c.
Temperature	40 - 65°C
Current density	200 - 300 ma/cm ²

The other⁽¹⁹⁾ was of the composition:

Orthophosphoric acid ($d = 1.69$)	40 v/o
Sulfuric acid ($d = 1.84$)	35 v/o
H_2O	25 v/o
Temperature	25°C
Voltage	6 V

In both cases the window technique was used; repeated masking of the window edges was required since preferential attack occurred in these regions. The cell arrangement used in electrothinning was as shown in Figure 6. When a very thin foil is produced, thinning is continued until holes begin to appear in the central region. Then the specimen is removed from the cell and washed first in distilled water and then in ethyl alcohol; both immersion washing and jet washing techniques are used. Small areas are cut from the foil and viewed in the electron microscope. A Hitachi HU-11 with tilt stage was employed.

6.

RESULTSa) Electron Microscopy

The observation of strain fields by using transmission electron microscopy was delayed for a considerable amount of time while we awaited the delivery of a tilt stage for the electron microscope. Since the arrival of this tilt stage the investigations have been carried out primarily into the Ni-ThO₂ system.

Specimens were examined for inclusion strain contrast effects by two complimentary methods. First, the selected area diffraction pattern was observed. The foil was tilted until a principal plane was normal to the beam. The specimen was then photographed in transmission since this orientation would fulfill the condition of a strong reflection operating in the plane of observation. Thus, if the strains were present, they should be in optimum orientation and will exhibit the diffraction contrast described in the previous theory section. The second method is to tilt the foil while examining it in transmission in order to watch for appearing contrast effects. Selected area diffraction will then reveal the orientation of the foil.

Figure 7 contains a transmission picture with several bend contours and the corresponding selected area diffraction pattern. The pattern shows that the plane of the foil is (112). For illustration, a discussion will be made of the solution

to this pattern. Three spots, A, B and C, are chosen and the distances OA, OB and OC are measured. OA = 2.7 cm., OB = 5.1 cm., and OC = 4.4 cm. The ratios are then taken and compared to the $(h^2 + k^2 + l^2)$ ratios of planes known to diffract in face centered cubic metals on a trial and error basis.

$$\frac{OC}{OB} = 0.863 \qquad \frac{(220)}{(311)} = \frac{2.828}{3.316} = 0.854$$

$$\frac{OC}{OA} = 1.63 \qquad \frac{(220)}{(111)} = \frac{2.828}{1.736} = 1.63$$

$$\frac{OB}{OA} = 1.89 \qquad \frac{(311)}{(111)} = \frac{3.316}{1.736} = 1.91$$

So the spots A, B and C are of the (111) (311) (220) form. By taking the cross product of any two of these then yields the zone axis, in this case of the $\langle 211 \rangle$ form. This means that the direction of the beam and the normal to the foil are $[211]$ and the plane of the foil is a (211) plane.

It is seen that, in this orientation, no diffraction contrast effects are evident which would indicate a strain field association with the particle matrix interface.

Figure 8 shows a foil with the right hand grain in a (112) orientation also. There are many small particles in the $\leq 200 \text{ \AA}$ range, but none of these exhibit strain diffraction contrast effects. It would be expected that perhaps the strain effects might recover in the larger particles

due to the larger vacancy source there; however, if the smaller particles are strained in the matrix, these are more likely to remain.

In Figure 9, the foil is seen to have cracked possibly during rolling. The orientation of the foil on either side of the crack is of the (111) form. The selected area diffraction pattern shows that some bending of the foil has occurred along the line of the crack so that the diffraction spots from either side do not coincide.

The lines in the transmission picture are thickness extinction contours and bend contours which are useful in that they provide a range of matrix diffraction contrast; then, if a weak diffraction effect is present it can be readily detected if a contour is superimposed on it thereby interacting with it. There are, in the regions marked with an X, very small particles in the 100 Å range which show the D-shaped lobes indicating a particle-matrix strain effect. It is suspected that these particles are at least partially coherent with the matrix, giving rise to the diffraction effect. The spotty rings in the diffraction pattern are from the thorium.

Figure 10 shows the plane of the foil in a (110) orientation. A large particle range exists in this area; however, no particle matrix strain effects are observed. Many extinction and bend contours are present, as in Figure 9, but the diffraction effect due to strain is clearly absent. Figure 11

is a higher magnification view of an area oriented in a (112) position where particles approximately 100 \AA and below are clearly seen. In this orientation, no diffraction contrast effects are seen.

Figure 12 shows another area in a (112) orientation. A small grain has begun to recrystallize at X and is interacting with the particles. Again, no evidence of strain field contrast effects are observed.

With respect to the deformation behavior of TD Nickel, the matrix does not seem to develop a preferred orientation with rolling. Using selected area diffraction, grains were found with all manner of orientations, (110) (111) (112) and even (100); furthermore, many grains had no principal plane parallel to the foil surface. The dispersed phase may have a great deal to do with this behavior. In Figure 13, the TD Nickel specimen was subjected to a 60% reduction in area by rolling. The diffraction pattern shows the asterism expected. The dislocation substructure is one of heavy tangles (denoted by X) which have interacted strongly with the particles. The particles have a great ability to impede dislocation motion in the lattice, even though, as can be seen in the picture, no strains are associated with the particle matrix interface.

It should also be noted that none of these particles have crushed or fragmented during rolling.

When annealed, the orientation of the recrystallized grains

are very often that of a (112) form. Figure 14 shows a recrystallized grain whose grain boundary is obviously held up by the thoria particles. Figure 15A shows a recrystallized grain growing in the scope from the heat of the beam. This ordinarily would not happen, but the combination of the hole acting as a growing site and a probable local condition of high stress began the recrystallization process. Figure 15B also emphasizes the high energy of recrystallization that must exist in order for the new grains to grow through the dispersed phase. The kinetics of recrystallization in these alloys must be much slower than those of pure nickel. Figure 16 shows a grain boundary which changes angle between grains at M and N; at N, the boundary is practically normal to the foil surface, whereas at M the angle is quite oblique. This is evidently due to the effect of the dispersed phase on the motion of the recrystallized grain.

D-shaped lobes have also been observed in $\text{Ni-}\gamma\text{Al}_2\text{O}_3$ alloys. A typical example is shown in Figure 17. At the time when this alloy was being examined, the tilt stage was not available and so a more complete investigation of this alloy could not be carried out.

b) X-Ray Line Broadening

Measurements of the shape of x-ray diffraction lines have been carried out using Ni- γ -Al₂O₃ alloys and the commercially obtained TD nickel. A Ni sample, prepared in a manner similar to the Ni- γ -Al₂O₃ alloys, has been used as a standard with which to measure the effect of instrumental (x-ray optical) broadening.

The preparation of the samples on which the x-ray measurements were carried out involved the alternate rolling and annealing of the extruded rod. Care had to be taken to avoid the introduction of a large degree of preferred orientation during this preparation as this would have caused certain of the diffracted lines to have too small an intensity to be readily measurable. Some difficulty was met due to the occurrence of fluorescence from the Ni and Ni alloy samples. The only available x-ray target which emits characteristic radiation which gives the required diffracted lines at sensible values of 2θ is the copper target. Unfortunately, copper radiation causes fluorescence of the nickel sample. Because of their similarity in wavelength, this radiation could not be separated from the CuK α radiation either by the use of filters or by varying the settings of the electronic counting equipment. This caused a high background intensity to exist.

All measurements were made using a Picker bi-plane diffractometer. In order to decrease the line broadening effects due to the instrument, this was used at a low take off angle. The

electronic counting equipment used with the diffractometer was adjusted to give the maximum peak-background ratio. The diffractometer was programmed so that it would count for periods of 400 secs. at intervals of $1/60^\circ$ (2θ) across the various diffraction lines. The results obtained in this way were then fed into a computer.

Initial experiments with the pure Ni standard indicated that, after annealing it at 700°C for a period of 5 hours, no broadening due to the sample could be detected.

The next step was to prepare samples of the two phase alloys on which we could carry out measurements of the interfacial strains. Our method of sample preparation introduced strains into all the matrix, not only into the interfacial regions. It was hoped to be able to anneal out these unwanted strains. The interfacial strains due to the existence of coherency or to the difference in thermal expansion of the two phases cannot, because of their nature, be removed by high temperature anneals. As yet, we have not succeeded in preparing specimens in which we believe that we have removed all but the interfacial strains. As will be described later, it seems necessary to use a different approach to the measurement of interfacial strains by the observation of x-ray diffraction line broadening.

7.

DISCUSSION

The presence of internal elastic strains has been detected by using both transmission electron microscopy and the broadening of x-ray diffraction lines. In the time available it has not been possible to carry out any quantitative measurements.

In the transmission electron microscopy of TD Nickel, the D-shaped lobes were only observed for small particles and when the foil was in the (111) orientation. A sufficiently large survey has not been carried out for us to be able to say emphatically that these are the only conditions under which these strains can be observed. The association of strains with smaller rather than larger particles would suggest, by comparison with precipitation hardened alloys, that they are coherency strains. The observation of strains in only one orientation would suggest an orientation dependence of these strains.

In the x-ray diffraction observations it seems probable that a large part of the observed line broadening is due to the existence of strains within the bulk of the matrix as opposed to those strains which are specifically associated with the particle interface. The existence of these strains in the bulk of the matrix is due to the existence of particles. They are, however, not the strains in which we are primarily interested.

In order to find the cause of the elastic strains, a different method of fabrication of samples for x-ray observation will have to be used. A thin foil of a dilute solid solution of the relevant element in nickel will be formed. This would then

be annealed to remove all internal strains. Internal oxidization would then be carried out. By this method we should eliminate those strains due to the body of the matrix. By varying conditions of internal oxidization, we will be able to vary the size and distribution of the dispersed phase and thus should be able to determine whether or not we are getting coherency. By varying the conditions of subsequent heat treatment, we should be able to detect the effects of differences in coefficient of expansion. It is expected that these and also the presence of dislocations would be the main cause of the existence of strains. Electron microscopy can be carried out using these same thin foils.

8.

REFERENCES

1. Becher, J. J., Trans. AIME, 209, 59 (1957).
2. Bean, C. P., and Livingston, J. D., App. Phys., 30, 1205 (1959).
3. Phillips, V. A., and Livingston, J. D., Phil. Mag., 7, 969 (1962).
4. Ashby, M. F., and Brown, L. M., Phil. Mag., 8, 1083 (1963).
5. Ashby, M. F., and Brown, L. M., Phil. Mag., 8, 1649 (1963).
6. Ansell, G. S., and Goodrich, R. S., to be published, Trans. AIME.
7. Howie, A., and Whelan, M. J., Proc. Roy. Soc., A, 263, 217 (1961).
8. Warren, B. E., Progress in Metal Physics, Vol. 8, p. 147 (1959).
9. Wagner, C. N. J., Acta Met. 5, p. 477 (1957).
10. Schoening, F. R. L., and Van Niekerk, J. N., Acta Met. 3, p. 10 (1955).
11. Mitchell, D., and Horn, F. D., Phil. Mag. 2, p. 15, (1957).
12. Warren, B. E., and Averbach, B. L., J. App. Phys. 21, p. 595 (1950).
13. Warren, B. E., and Averbach, B. L., J. App. Phys. 23, p. 1059 (1952).
14. McKeehan, M., and Warren, B. E., J. App. Phys. 24, p. 52 (1953).
15. Kelly, A., and Nicholson, R. B., Prog. Mat. Sci., Vol. 10, p. 149 (1963).
16. Thirsk, and Whitmore, Trans. Farad Soc., 36, p. 565, (1940).
17. Bonis, L. J., and Grant, N. J., Trans. AIME, 224, p. 308 (1962).

18. Ansell, G. S., Private Communication.
19. Goodrich, R. S., Private Communication.

TABLE I

COMPOSITION AND STRUCTURAL DATA ON INTERNALLY OXIDIZED NICKEL ALLOYS

Solute Wt. %	Volume % oxide*	Int. Oxidation time, hours	Particle Size		Interparticle Spacing	
			Radius, Range**	Angstroms Av.	Range***	micron Av.
1.25 Al	5.58 Al ₂ O ₃	51	100-500	200	0.1-0.5	0.25
2.27 Al	10.44	60	100-1,800	500	0.5-1.5	0.75
2.05 Ti	6.4 TiO ₂	67	150-2,000	650	0.5	0.5
3.08 Ti	7.8	81	1,000-10,000	3,500	1-5	2.5
1.17 Si	10.5 SiO ₂	48	200-5,000	1,000	0.5-2	0.9
2.25 Si	21.0	57	1,000-10,000	3,500	1-5	2.5

* Internally oxidized at 750°C

** By electron microscope

*** Between oxide clusters

<i>Ni</i>	<u>STRUCTURE TYPE</u>	<u>LATTICE CONSTANT</u>
	<i>A1</i>	$a_{Ni} = 3.524 \text{ \AA}$

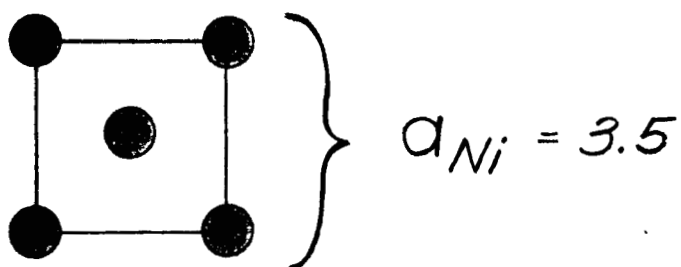


FIG 1

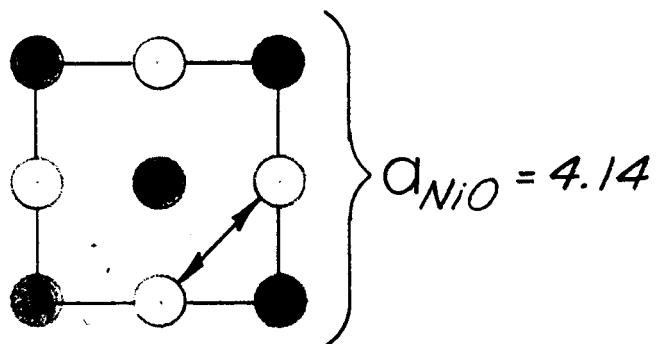
THE CRYSTAL STRUCTURE OF Ni

NiO STRUCTURE TYPE LATTICE CONSTANT

B1

$$a_{NiO} = 4.14 \text{ \AA}$$

O-O DISTANCE



$$\frac{2.91 \text{ \AA}}{\left(\frac{a_{NiO}}{2} \cdot \sqrt{2} \right)}$$

FIG 2

THE CRYSTAL STRUCTURE OF *NiO*



STRUCTURE TYPE

LATTICE CONSTANT

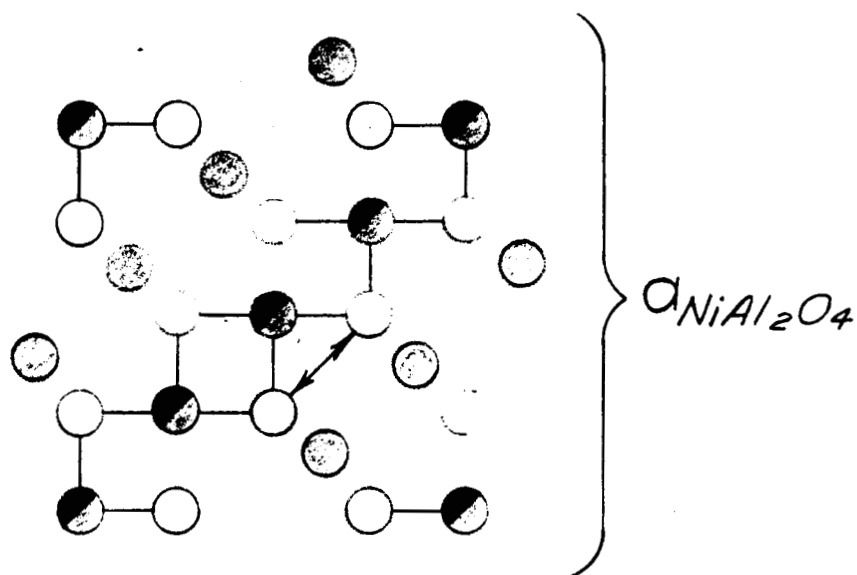
INVERSE SPINEL
ONLY Ni WITH
INVERSE SPINEL
 $\text{Al}(\text{NiAl})_2\text{O}_4$

$$a = 8.046 \text{ \AA}^{\circ}$$

NiAl_2O_4



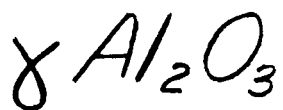
O-O DISTANCE



$$\frac{2.84 \text{ \AA}^{\circ}}{\left(\frac{a_{\text{Al}(\text{NiO}_4)} \sqrt{2}}{4} \right)}$$

FIG 3

THE CRYSTAL STRUCTURE OF NiAl_2O_4



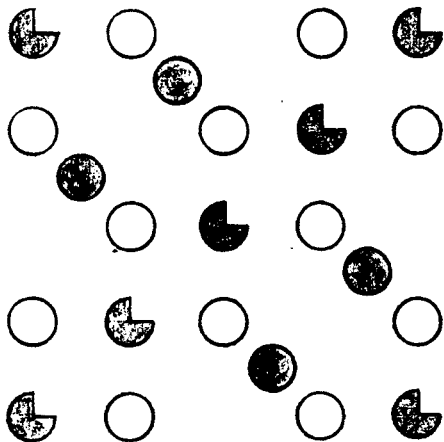
STRUCTURE TYPE

LATTICE CONSTANT

SPINEL DEFECT
Al_{2.66} O₄

$$a = 7.92 \text{ \AA}$$

O-O DISTANCE



$$\left(\frac{\frac{2.80 \text{ \AA}}{a_{\text{Al}_2\text{O}_3} \cdot \sqrt{2}}}{4} \right)$$

FIG. 4

THE CRYSTAL STRUCTURE OF $\gamma \text{Al}_2\text{O}_3$

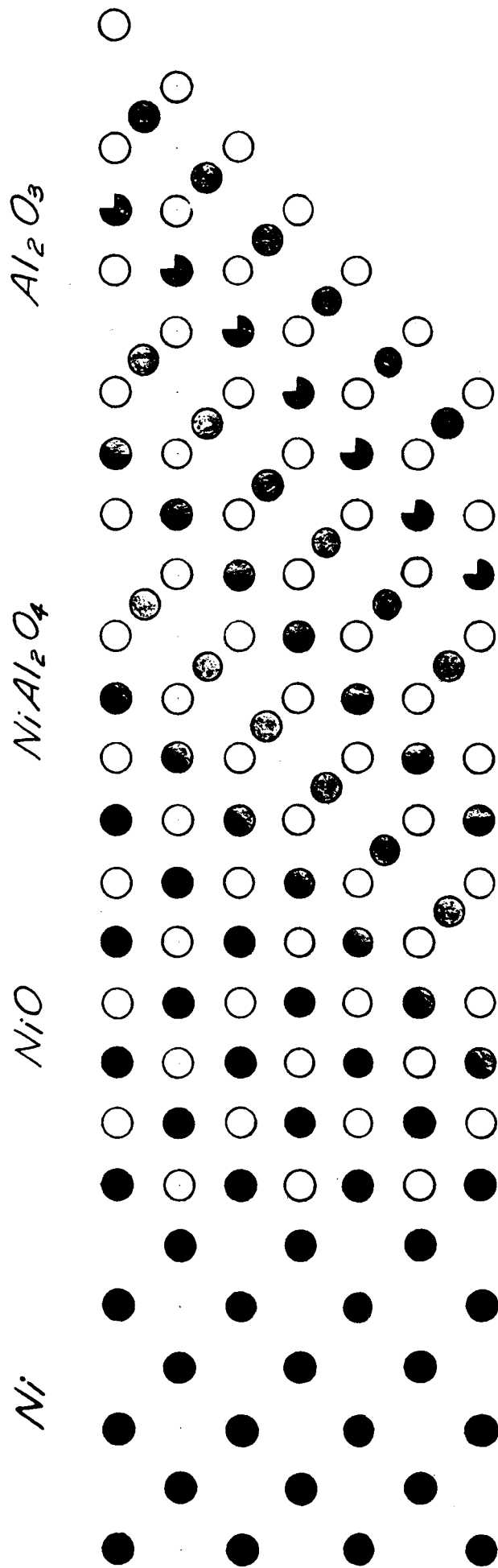


FIG 5 THE COHERENT TRANSITION FROM Ni TO Al_2O_3 (γ)

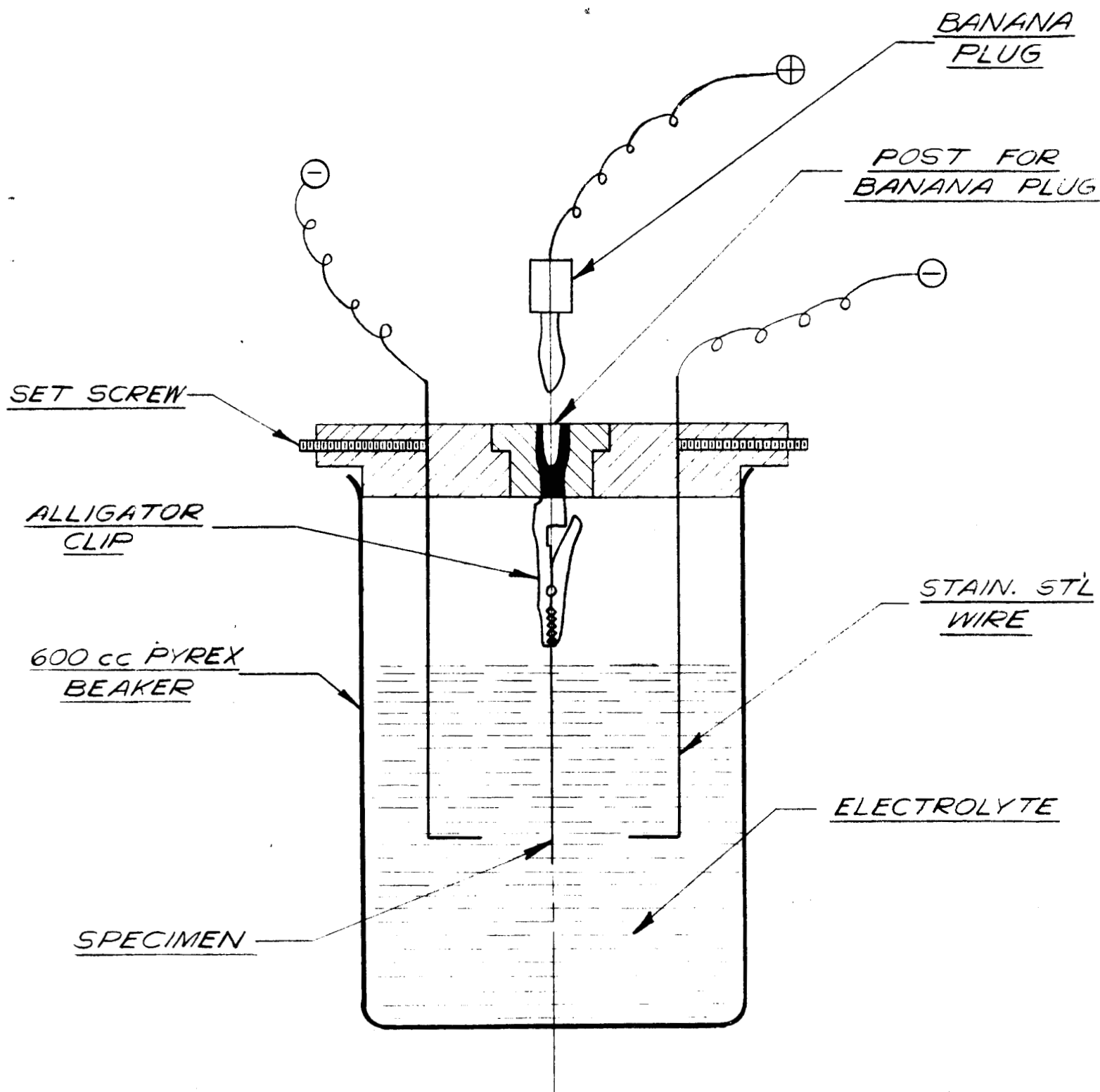


FIG. 6 ELECTRODE ASSEMBLY FOR ELECTRO-POLISHING PROCESS

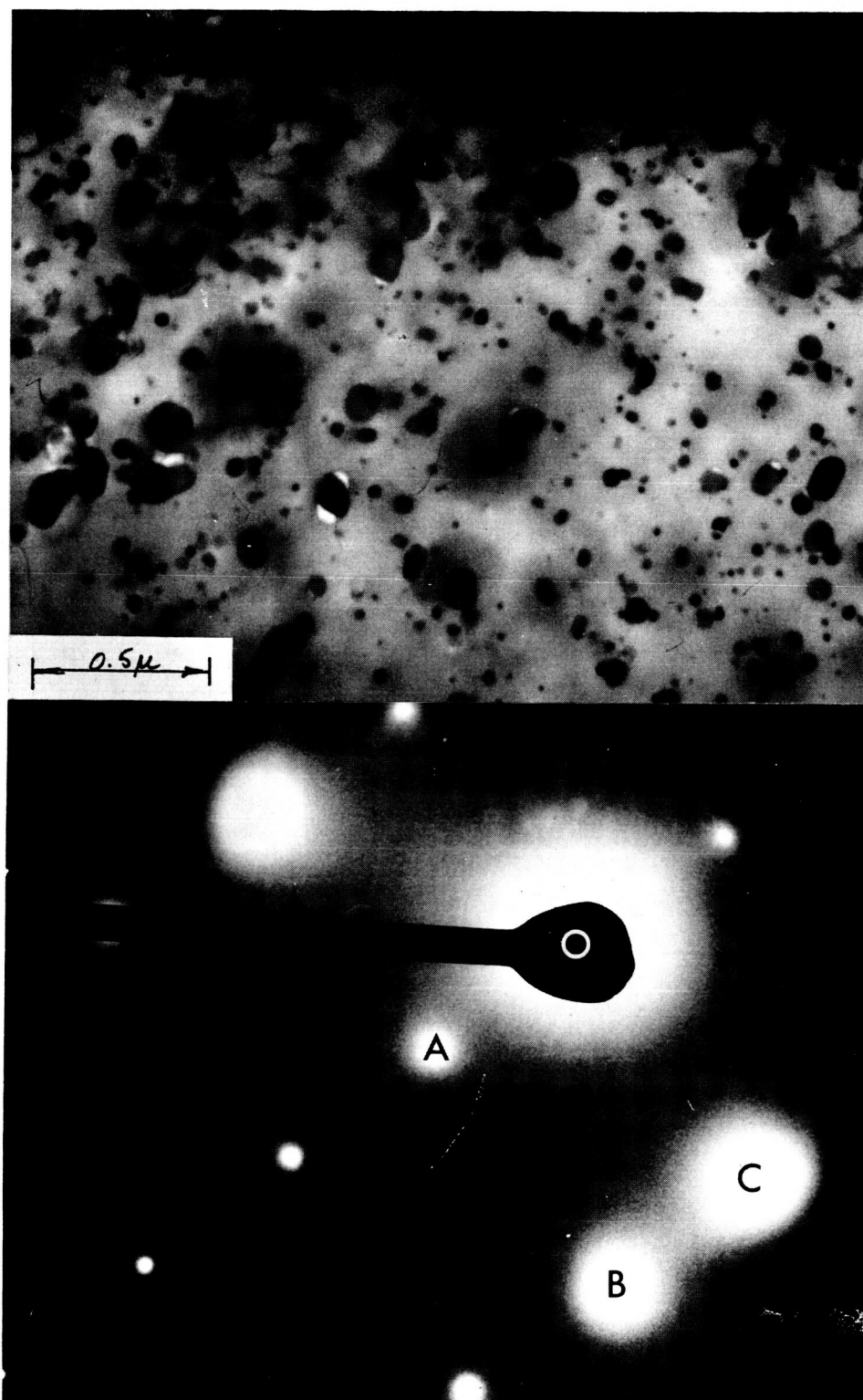


FIGURE 7

Annealed TD Nickel

Plane of the foil is of the (112) form where A, B, and C are (111) (131) and (220) respectively. No diffraction contrast indicating strain fields associated with the particle-matrix interface is observed.

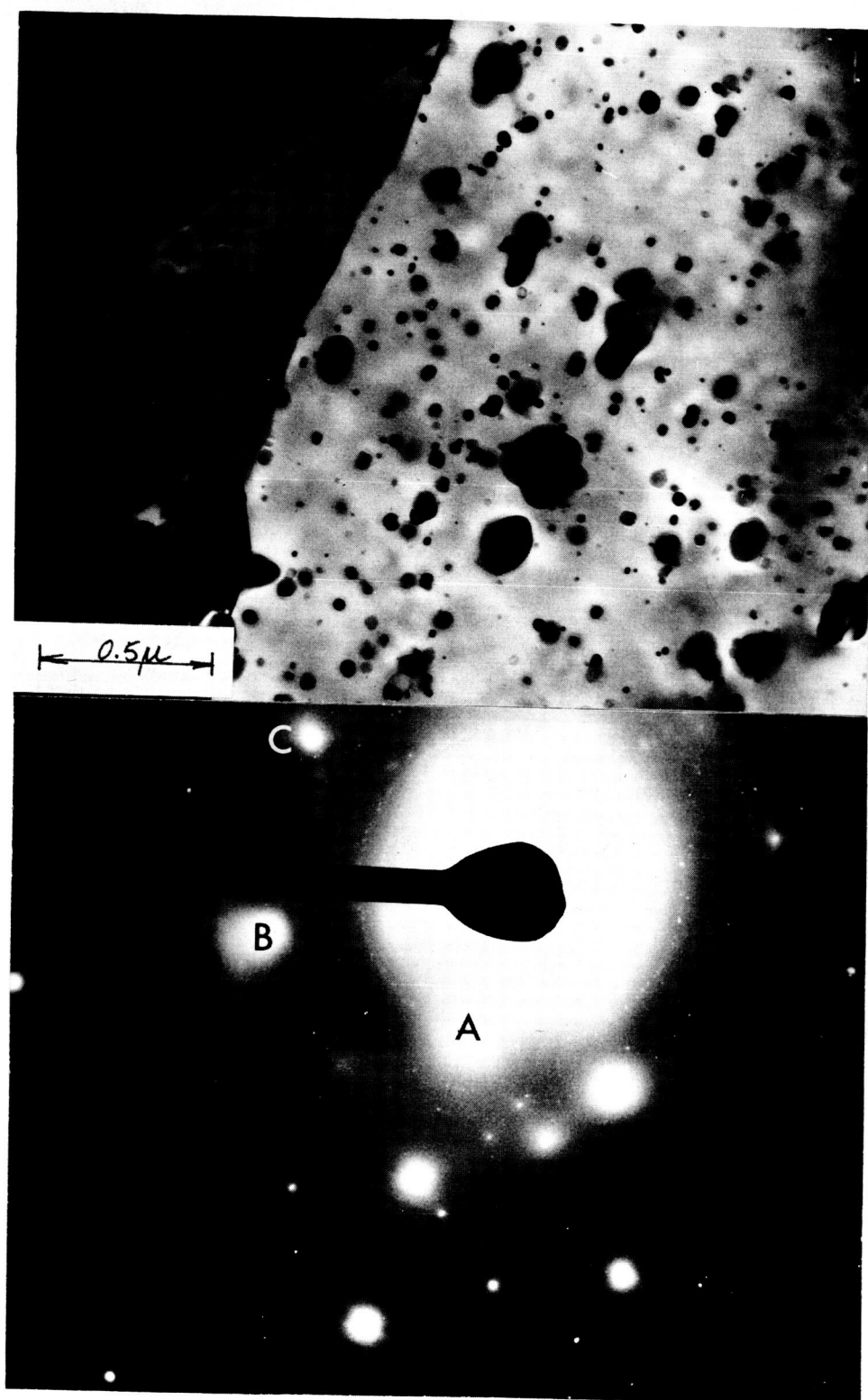


FIGURE 8

Annealed TD Nickel

Diffraction pattern shows a (112) orientation of the foil. The pattern corresponds to the grain at the right.

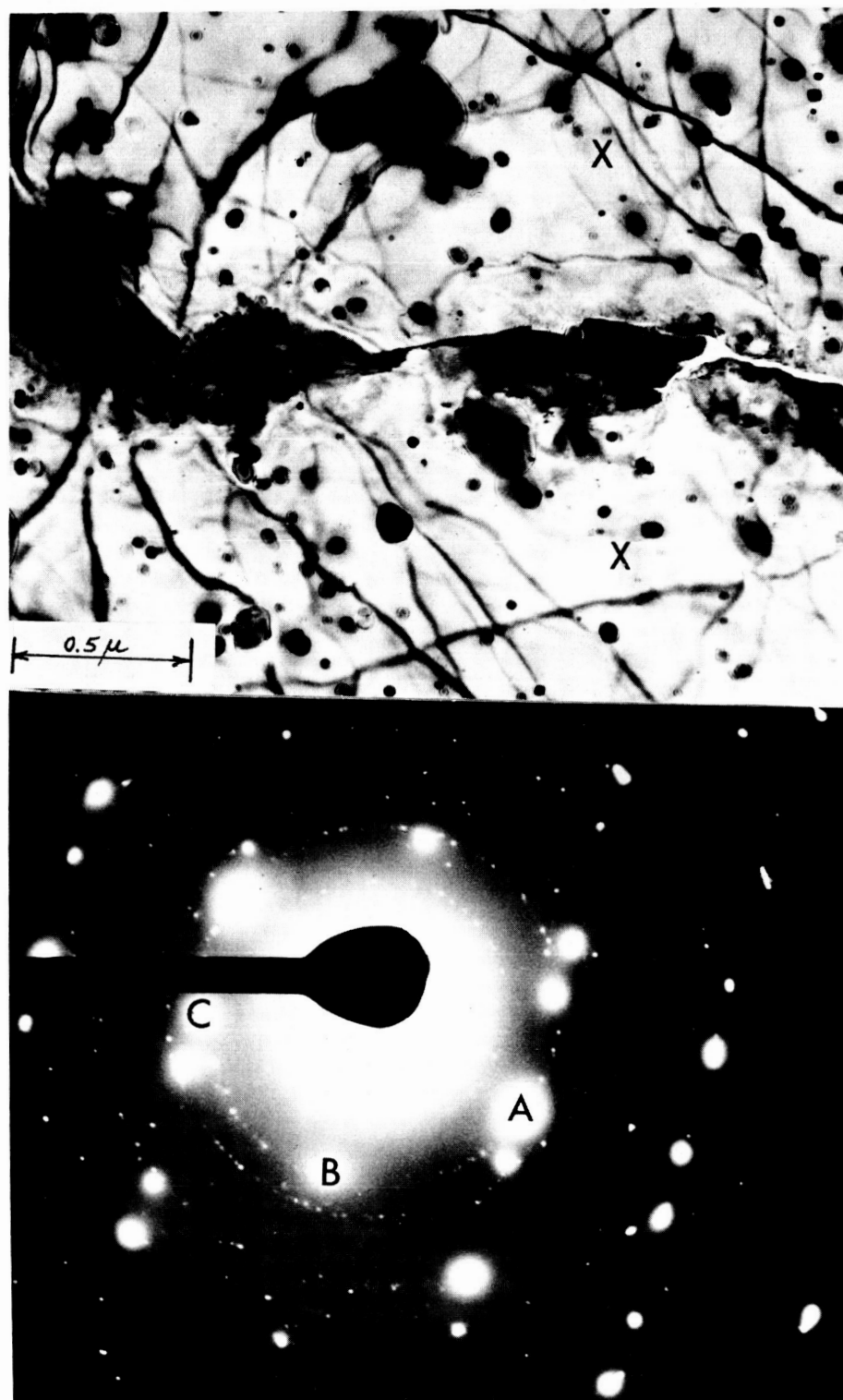


FIGURE 9

Annealed TD Nickel

A, B and C are all of the (220) form and the plane of the foil is (111). The double spots are due to the foil bending along the line of the crack. Very small particles (X) in the 100 Å range exhibit diffraction contrast typical of a strained interface.

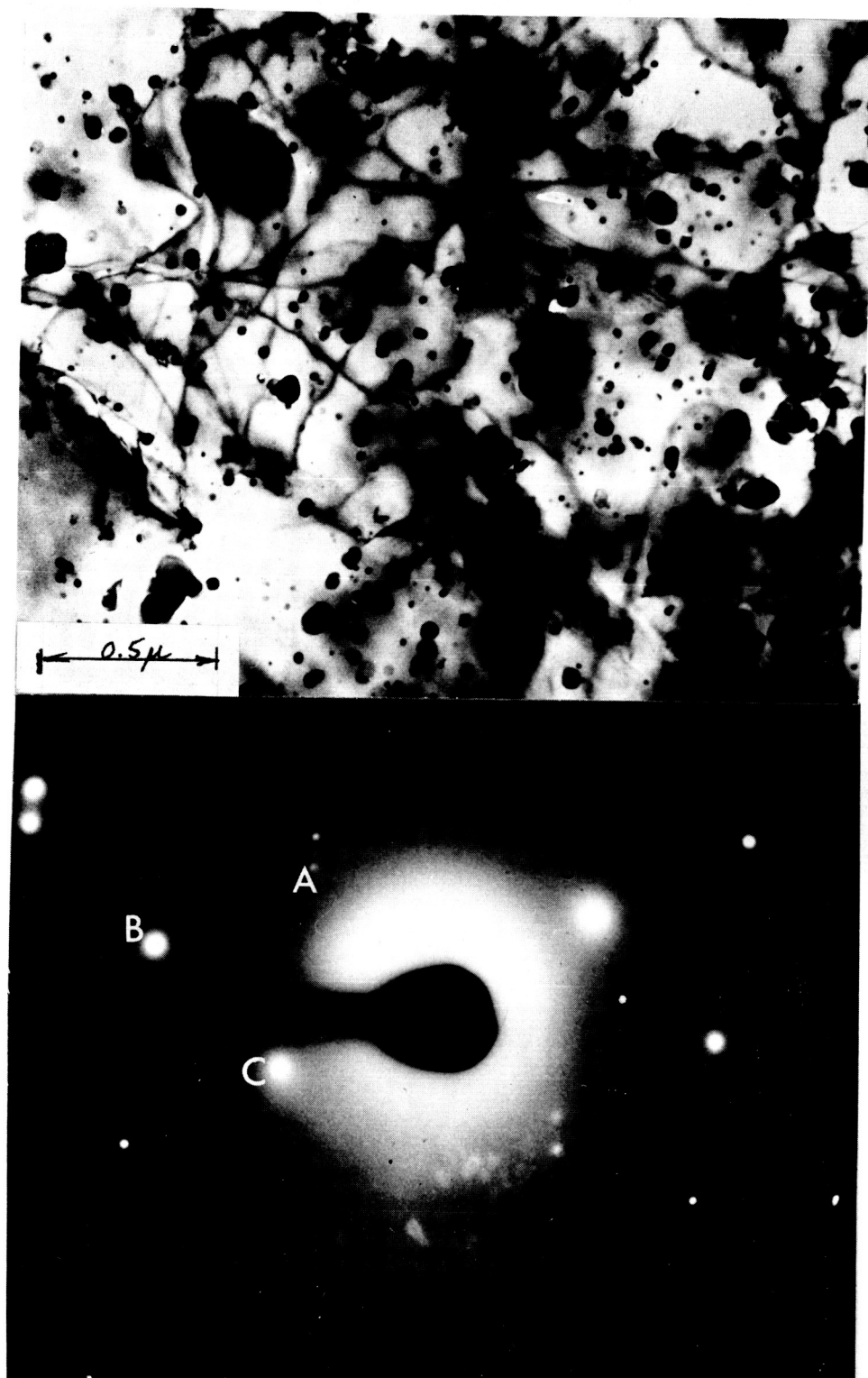


FIGURE 10

Annealed TD Nickel

A, B and C are (111) (022) and (111) respectively and the plane of the foil is of the (110) form. A slight rotation around a (100) direction has taken place.

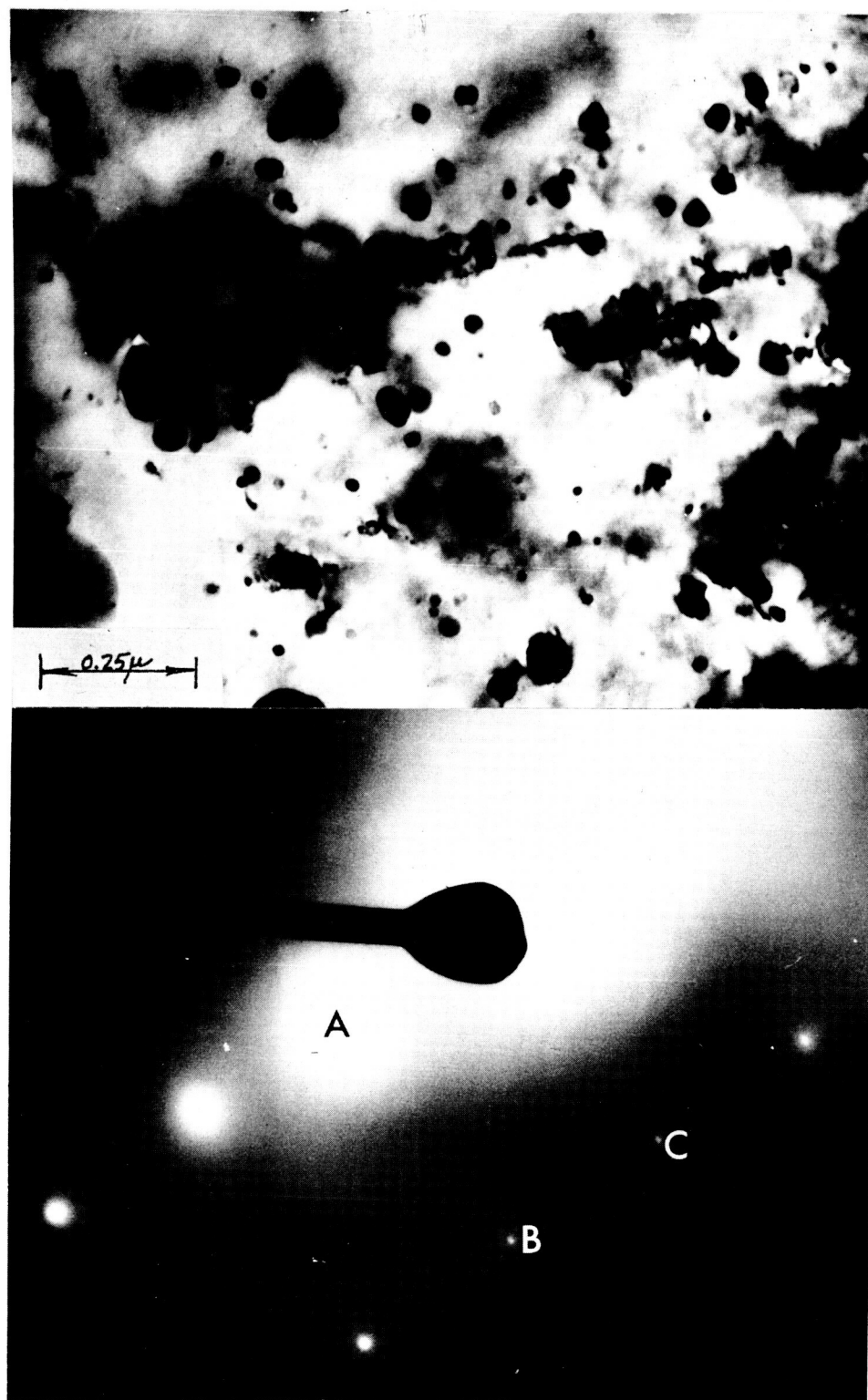


FIGURE 11

Annealed TD Nickel

A, B and C are (220) (311) and (111) respectively. The plane of the foil is in a (112) orientation. This higher magnification shot clearly shows particles in the 100 Å range.

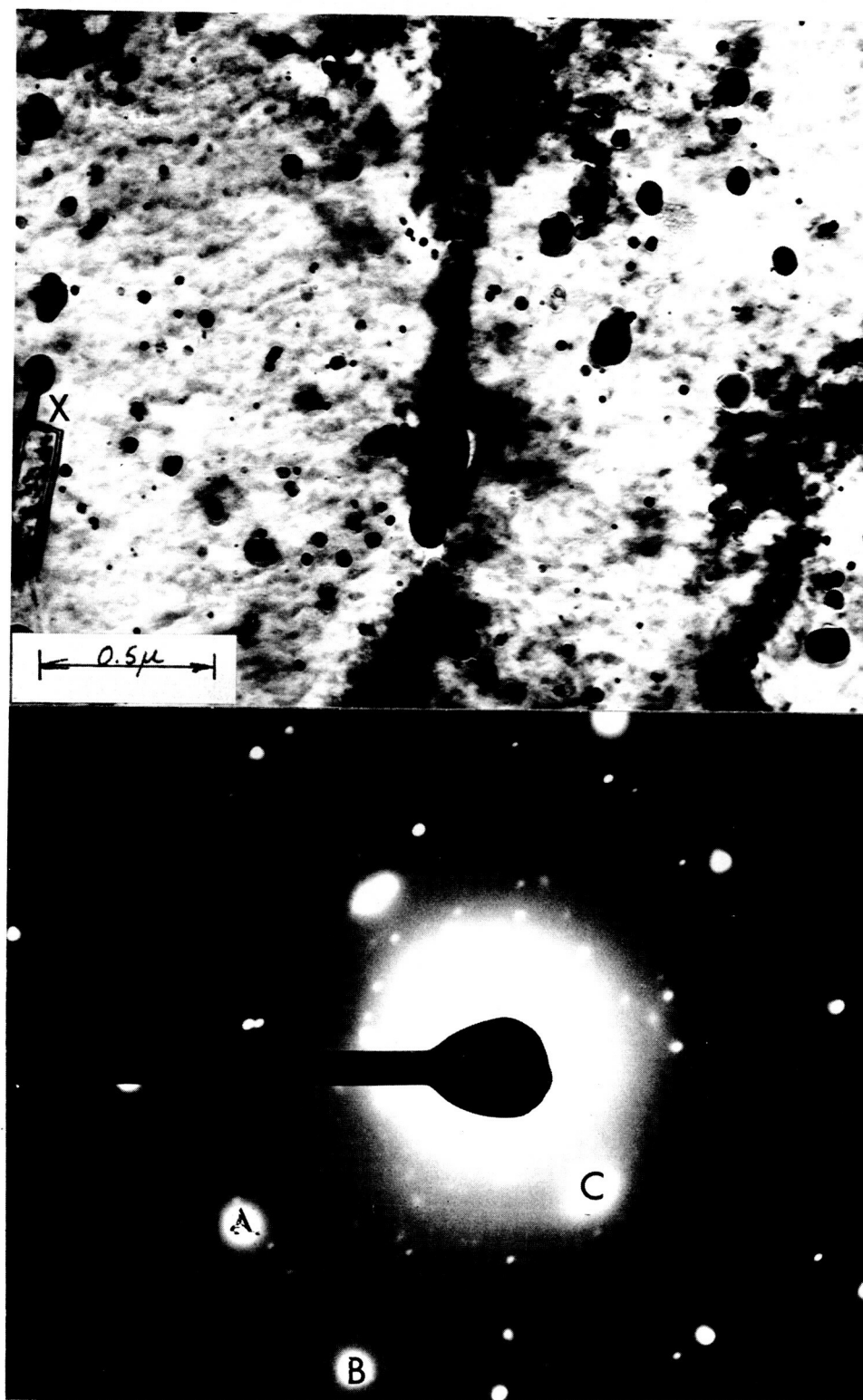


FIGURE 12

Annealed TD Nickel

A, B and C are (220) (311) and (111) respectively. The foil surface is of the (112) form and spots are present from the Thoria particles. At X, a small grain is seen to interact with several particles.

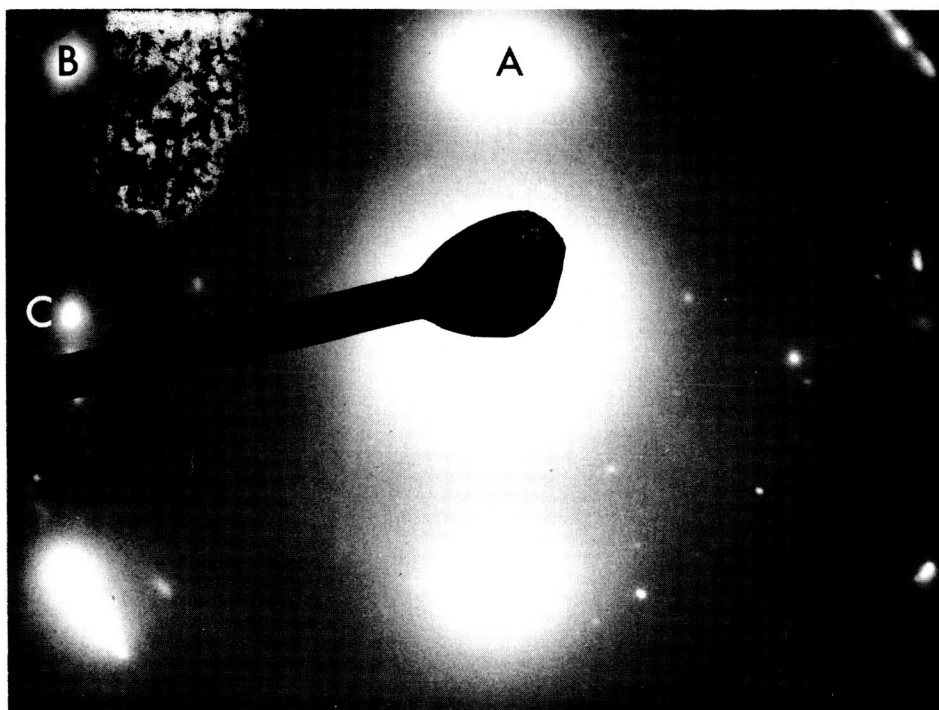
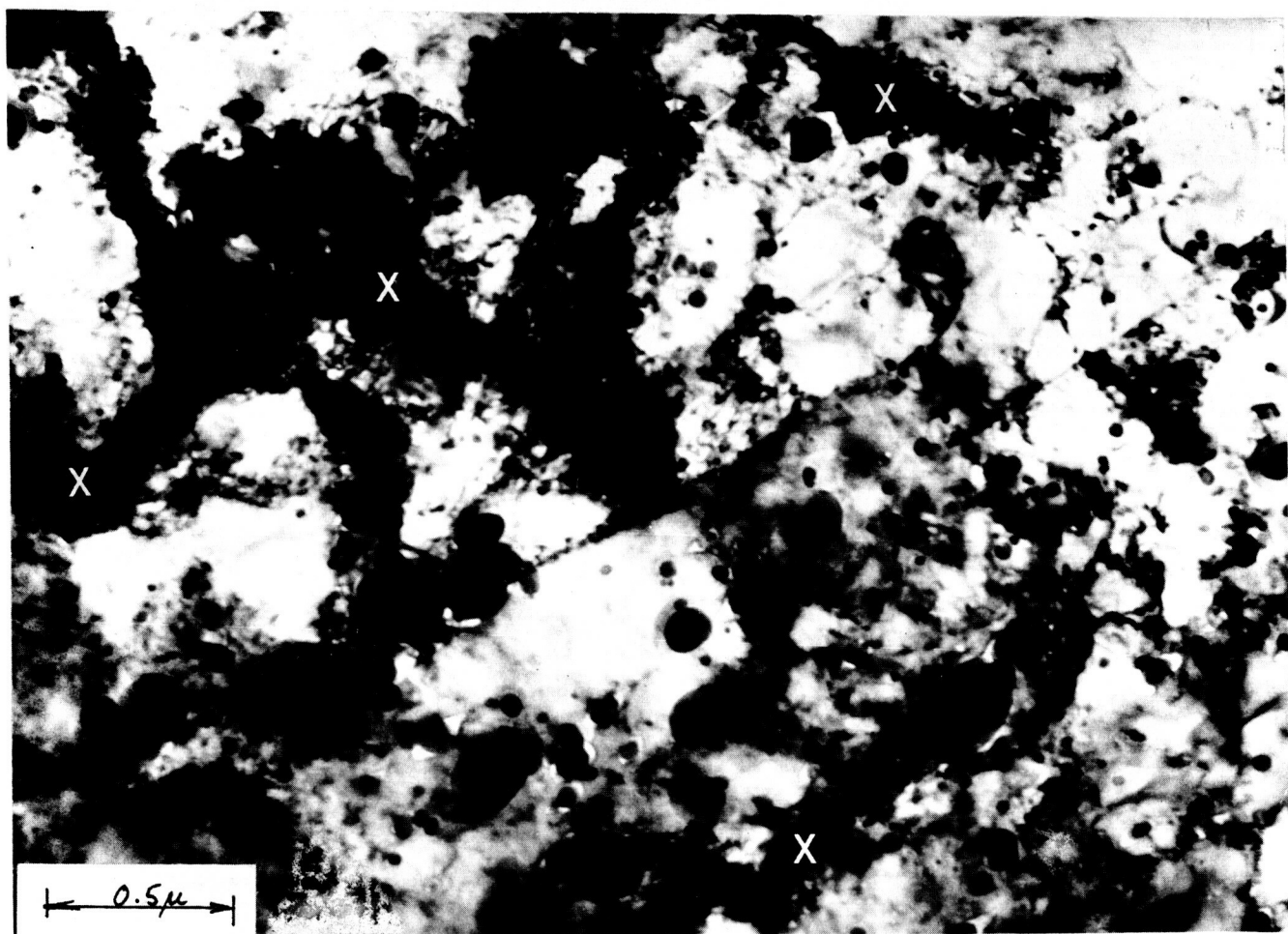


FIGURE 13 TD Nickel, rolled 60% reduction in area.
Plane of the foil is (112). Dislocation
tangles denoted by X.

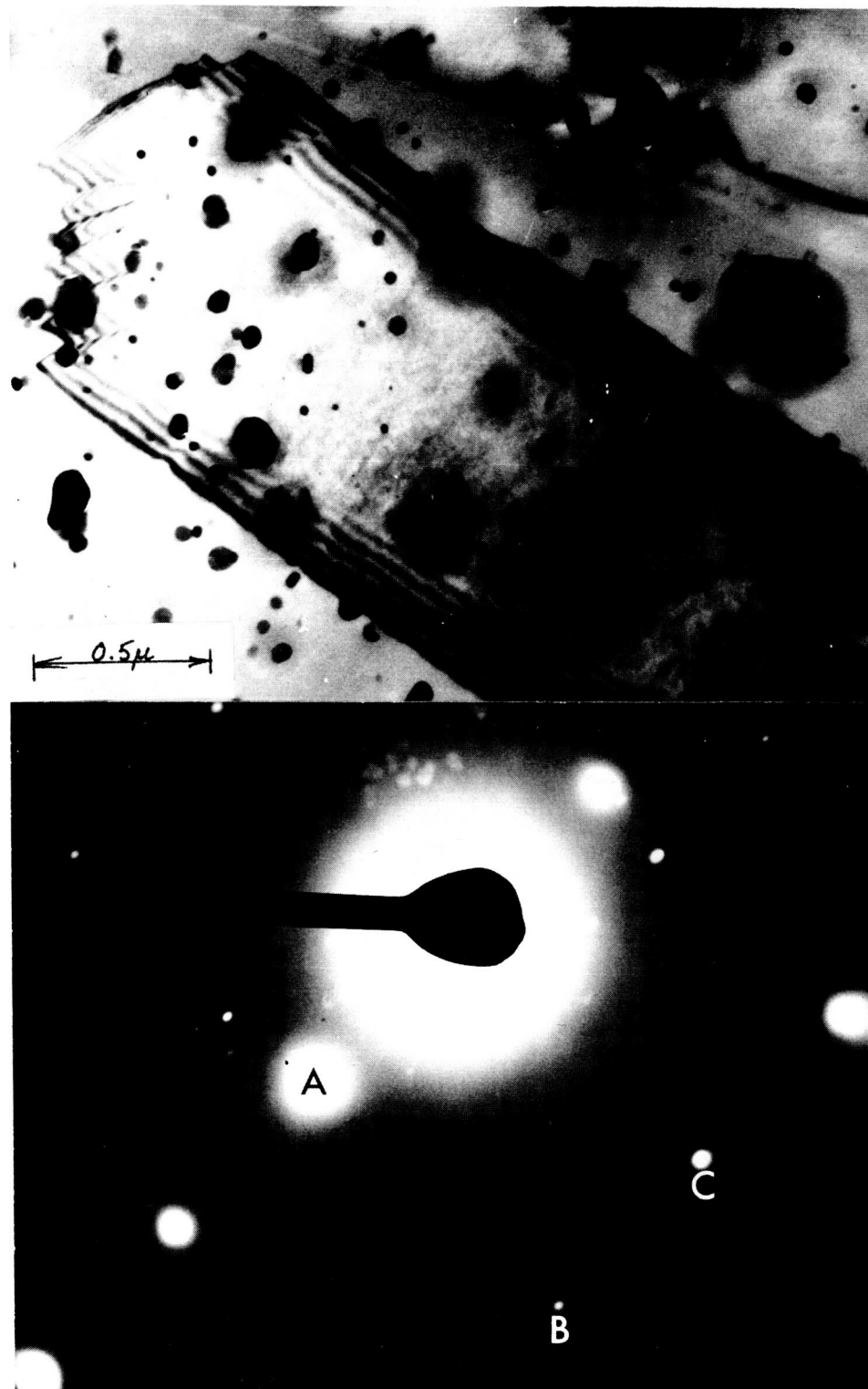


FIGURE 14

Annealed TD Nickel

View of recrystallized grain of a (112) form growing in matrix. Selected area diffraction is of the recrystallized grain only.



FIGURE 15

A and B

- A) Recrystallized grain growing from hole.
- B) Recrystallized grain interacting with particles.

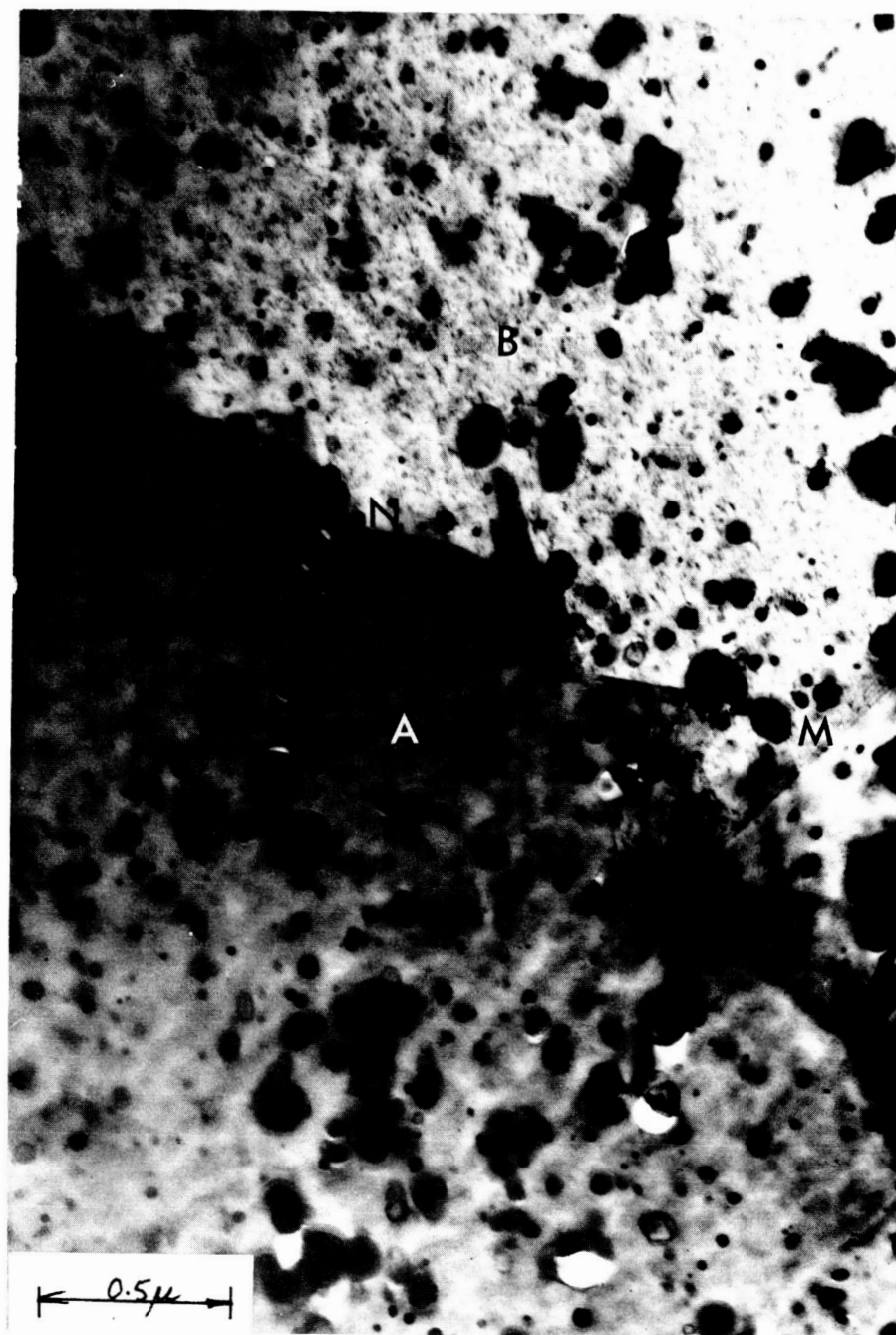


FIGURE 16

Annealed TD Nickel - Grain Boundary

Recrystallized grain A which grew into grain B.



FIGURE 17

Ni - 5.5% Al

55,000X

Contrast effects indicating strain fields
are seen at the points marked X